

Chapter 6

Systematic Uncertainties

6.1 Introduction

There were two classes of systematic uncertainties for $P_\mu^\pi \xi$: those related to the accuracy of the P_μ simulation, and a separate group that were derived from the degree to which the decay positron reconstruction treated the data and simulation in the same way. The reconstruction systematic uncertainties were evaluated simultaneously for ρ , δ and $P_\mu^\pi \xi$, by exaggerating an effect in the simulation or the analysis software; the exaggerated spectrum was then fit against the original spectrum to determine the change in the muon decay parameters (MPs). The exaggeration factors were made as large as possible to obtain a statistically meaningful MP change, while maintaining a linear relationship with the MPs. The change in MP and its uncertainty were scaled down according to how large the effect could actually be, resulting in a “sensitivity”. When the exaggerated and original spectrum were highly correlated (*i.e.* they contained a large number of events with identical energy and angle), the uncertainties in the MP differences were rescaled so that the reduced χ^2 from the fitting procedure was equal to one.

6.2 Overview

The $P_\mu^\pi \xi$ uncertainties are summarised in Table 6.1, from which it is clear that the measurement is limited by the accuracy of the muon beam and the solenoidal fringe field. The table indicates three statistical uncertainties; these could have been reduced by accumulating more data and/or simulation under the same running conditions. The most recent TWIST analysis (MacDonald '08 in the table) did not re-evaluate the polarisation uncertainties, since it was a measurement of ρ and δ . A selection of the systematic uncertainties were set dependent, and in these cases Table 6.1 contains the uncertainty for the nominal sets only.

Table 6.1: Summary of $P_\mu^\pi \xi$ uncertainties. The statistical uncertainties are marked (stat.); otherwise the uncertainties are systematic. For this analysis, (0) indicates the uncertainty is no longer evaluated.

Category	Thesis section	New eval.?	Uncertainty ($\times 10^{-4}$)		
			This analysis	MacDonald '08 [10, 18]	Jamieson '06 [21, 57]
Extraction of $\Delta P_\mu^\pi \xi$ (stat.)	7.1	✓	2.4*	3.7	6
Polarisation					
Production target	6.3.1	✓	0.4	2.1	2.1
μ^+ beam/ fringe field	6.3.2	✓	21.5	34.0	34.0
Stopping material					
λ (stat.)	6.3.3	✓	3.0	Not eval.	Not eval.
$P_\mu(t)$ model	6.3.3	✗	(0)	12	12
Background muons	6.3.4	✓	1.0	2	1.8
Beam intensity	6.3.5	✓	*	0.2	1.8
Chamber response					
DC STR	6.4.1	✓	0.0	6.0	Not eval.
Wire time offsets	6.4.2	✓	*	0.4	8.9
US-DS efficiency	6.4.3	✓	*	1.1	1.9
Dead zone	6.4.4	✓	*	0	0.1
Foil bulge	6.4.5	✗	(0)	0.7	2.2
Cell asymmetry	6.4.6	✗	(0)	0	2.2
Density variations	6.4.7	✗	(0)	0.2	0.2
Alignment					
z length scale	6.5.1	✗	0.7	0.7	2.2
u/v width scale	6.5.2	✗	0.2	0.2	Not eval.
DC alignment	6.5.3	✗	0.02	0.02	2.2
B-field to axis	6.5.4		*	Not eval.	0.3
Positron interactions					
δ -electron rate	6.6.1	✓	*	1.4	2.9
Bremsstrahlung rate	6.6.2	✓	*	0.03	
Outside material	6.6.3	✓	*	0.6	0.2
Multiple scattering	6.6.4	✗	(0)	0	0.8
Energy loss	6.6.5	✗	0.01	0.01	0.1
Resolution	6.7	✗	0.7	0.7	Not eval.
Momentum calibration					
Tracking B-field	6.8.1	✓	*	1.1	0.9
Kinematic endpoint					
Parameters (stat.)	6.8.2	✓	*	0.5	1.6
Propagation	6.8.2	✓	*	0.09	
External					
Radiative corrections	6.9.1	✗	0.5	0.5	1.0
η correlation	6.9.2	✗	1.1	1.1	Not eval.

6.3 Polarisation

6.3.1 Production target

The simulation generated muons with anti-parallel spin and momentum vectors, starting from the end of the M13 beam line. This neglected multiple scattering in the graphite production target and the beam line vacuum window, which changed the momentum vector but not the spin. This is treated here as a systematic correction with an associated uncertainty. (The difference in precession frequencies of the momentum and spin through the M13 beam line is neglected since it introduced an error of $< 10^{-8}$; see Appendix I).

Surface muons are produced with $p \approx 29.79 \text{ MeV}/c$, but the beam line was nominally tuned to accept muons with an average momentum of $\langle p \rangle = 29.6 \text{ MeV}/c$. Therefore the muons lost an average momentum of $0.19 \text{ MeV}/c$, which is equivalent to $\approx 3.8 \text{ mg}/\text{cm}^2$ in graphite. The width of the resulting multiple scattering distribution, θ_0 , was estimated using a **GEANT4** simulation. As a consistency check, the same estimate was made using an approximate expression from the Particle Data Group (PDG)[3], and two further approximations from Ref. [99] that are intended to be more accurate than the PDG. The results for θ_0 varied from 8.2 mr to 12.0 mr , and are shown in Table 6.2. The degree to which the spin is depolarised with respect to momentum is then estimated by $\cos(\theta_{\text{space}}^{\text{rms}})$, where $\theta_{\text{space}}^{\text{rms}} = \sqrt{2} \theta_0$. The central value of the correction was taken as the **GEANT4** result, since it was believed to be the most accurate of the estimates. The uncertainty in the correction was half of the range of the four θ_0 estimates.

The evaluations were repeated for the lower momentum sets at $\langle p \rangle = 28.75 \text{ MeV}/c$ and $\langle p \rangle = 28.85 \text{ MeV}/c$, and these results are included in Table 6.2. Later the consistency of $\Delta P_{\mu}^{\pi} \xi$ between the nominal and lower momentum sets (after correction) will be demonstrated.

These estimates did not include the $3 \mu\text{m}$ beam line vacuum window that the muons passed through. This was safely neglected since it corresponded to just $0.3 \text{ mg}/\text{cm}^2$ of material, which is an order of magnitude less than the average material traversed in the production target.

The previous $P_{\mu}^{\pi} \xi$ analysis found a systematic uncertainty of 2×10^{-4} due to depolarisation in the production target; this was evaluated as a conservative upper limit, rather than making a correction[57].

Table 6.2: $\Delta P_{\mu}^{\pi\xi}$ correction due to multiple scattering within the graphite production target. The uncertainty is estimated from the spread of θ_0 values from the four estimates.

Beam tune	Lower momentum		Nominal
Beam line $\langle p \rangle$ (MeV/c)	28.75	28.85	29.60
Momentum loss in graphite (MeV/c)	1.04	0.94	0.19
Graphite thickness ^a			
(mg/cm ²)	18.9	17.2	3.8
($\times 10^{-4} X_0$) ^b	4.43	4.03	0.89
Scattering distribution width, θ_0 (mr) ^c			
GEANT4	24.2	22.9	9.3
Simple PDG estimate[3]	25.3	24.0	10.4
Eq. (6) of Ref. [99]	28.9	27.4	12.0
Eq. (7) of Ref. [99]	22.8	21.5	8.2
$\Delta P_{\mu}^{\pi\xi}$ correction ($\times 10^{-4}$)	-5.9 ± 1.6	-5.2 ± 1.4	-0.9 ± 0.4

^a The range estimate assumed only ionisation energy losses, and used the Bethe-Bloch formula in the continuous slowing down approximation.

^b X_0 = one radiation length (42.7 g/cm² for graphite).

^c θ_0 is the standard deviation of a Gaussian fit to the central 98% of the the plane-projected multiple scattering distribution.

6.3.2 Muon beam and fringe field

Overview

The simulation transported the muon spin from the end of the M13 beam line to the stopping target. The leading $P_\mu^\pi \xi$ uncertainty is derived from the accuracy of the magnetic field map that was used in the simulation, and the muon beam measurement that the simulation was provided with. Uncertainties from the muon beam measurement are separated into two approximately orthogonal parts: the average position and angle of the beam, which is dominated by the reproducibility of the time expansion chambers (TECs), and the angular resolution, which has contributions from aging of the TEC sense planes, noise from the TEC electronics, and the simulation of multiple scattering within the TEC modules.

In the following discussion, $P_\mu(0)$ is the z -component of the polarisation for thermalised muons *before* any time dependent depolarisation has taken place. The term “fringe field” refers to the solenoidal magnetic field from the end of the M13 beam line ($z \approx -200$ cm), up to the first drift chamber ($z \approx -50$ cm), which fully determines the beam’s $P_\mu(0)$. Also, the estimate of this uncertainty assumes that the reader is familiar with the solenoidal magnet (Section 2.7), the measurement of the magnetic field map (Appendix D), the parameters of the muon beam inside the detector (Section 3.7), and the available data sets (Section 5.3).

Validation of spin tracking

A contribution to the systematic uncertainty comes from the two sets that used steered muon beams. These sets had a lower $P_\mu(0)$ since their beams were deliberately steered away from the solenoid’s symmetry axis, into regions where the transverse field components were larger; the TEC measurements for these sets were described in Fig. 5.2. From the data, a spectrum fit between the nominal and steered sets finds

$$\Delta P_\mu^{74-76}(0) = (101 \pm 8) \times 10^{-4}, \quad (6.1)$$

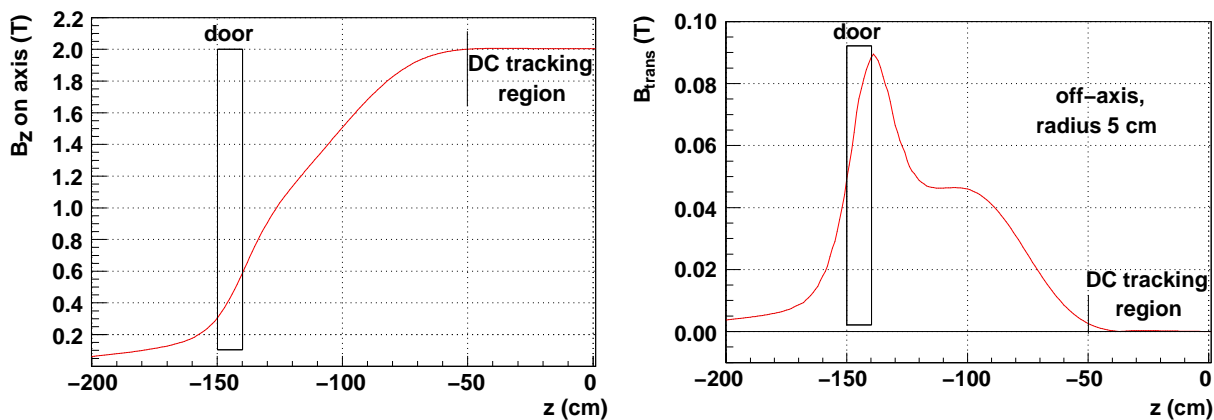
$$\Delta P_\mu^{87-86}(0) = (59 \pm 7) \times 10^{-4}, \quad (6.2)$$

where the superscripts (74-76) and (87-86) refer to the set numbers in Table 5.1. The degree to which the simulation reproduces these large differences will contribute to the systematic uncertainty from the field and muon beam. From here on, these quantities will be referred to as ΔP_μ^{74-76} and ΔP_μ^{87-86} .

Fringe field

The on-axis longitudinal field component and *off-axis* transverse components of the “production” fringe field map³⁵ are shown in Fig. 6.1; the on-axis transverse components were negligible. The longitudinal field component increases throughout the region between the door entrance and the DC tracking region. The transverse components start to increase about 10 cm before the yoke door, and are maximised just inside the door.

The resulting polarisation of a nominal and steered beam as a function of z are shown in Fig. 6.2(a). The polarisation is almost unchanged until the door ($z = -150$ cm), at which point it starts to undergo depolarisation that continues until the first drift chamber ($z = -50$ cm). The quality of the fringe field downstream of the door is important since it controls the rate of depolarisation. The field upstream of the door is also important since it affects which part of the fringe field the beam is transported through. The average x -positions of the same beams are shown in Fig. 6.2(b). The steered beam passes through a part of the fringe field with larger transverse field components, resulting in a significantly greater depolarisation.



(a) B_z component, on-axis ($x = y = 0$).

(b) Transverse \vec{B} component at 5 cm radius.

Figure 6.1: Fringe field components from OPERA.

The B_z components of the fringe field were measured with five Hall probes. A field map was then generated using the OPERA software package[83], and this map was used for the analysis. The inputs to OPERA (*e.g.* coil positions and radii, current density, B-H curves, door position) were adjusted to minimise discrepancies with the measured field map. The

³⁵This is the map that was used to generate all the simulations, and to analyse both the data and simulation.

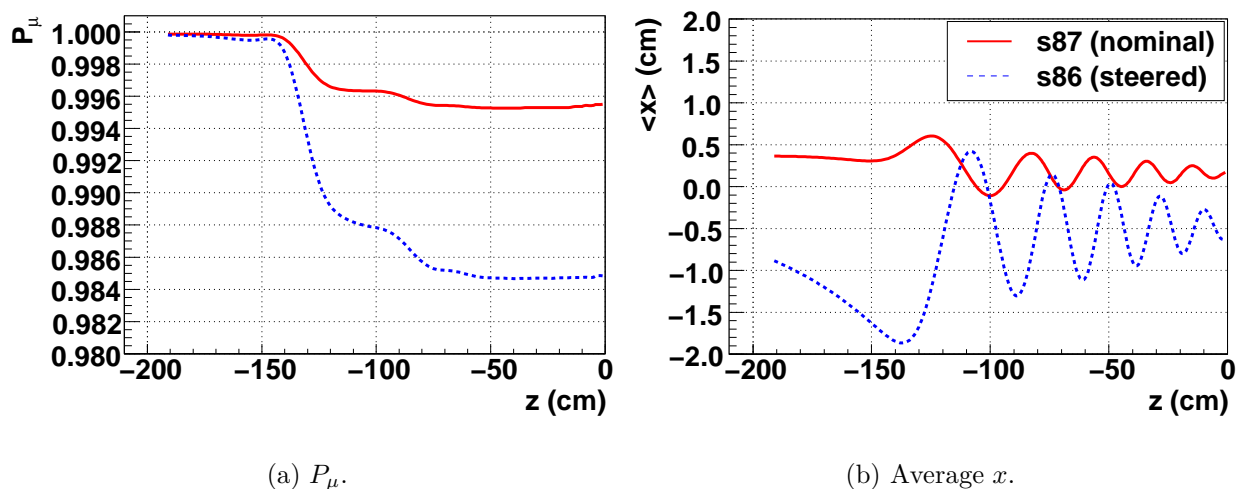


Figure 6.2: Polarisation and mean position for a nominal and steered beam.

Hall probe measurements had known deficiencies: they were precise to 0.1 mT, but there is evidence that they were only accurate to about 0.9 mT³⁶; the Hall probes were single axis, and only recorded the B_z field component; the probes were attached to an arm that sagged under gravity, introducing a vertical misalignment of up to 0.1 cm. Also, the whole mapping device was aligned in the yoke coordinate system to about 0.2 cm in x and y .

The OPERA simulation also had known deficiencies: the steel in the floor of the M13 area and the final M13 quadrupoles were not included in the field map used for production; there were no measurements of the B_x and B_y components to validate the finite element method used in OPERA; and comparison with the Hall probe results could not produce a precise translational alignment. As a result of the deficiencies in the Hall probe and OPERA maps, the B_z components did not agree (see Fig. 6.3). After the production simulations were produced, an improved fringe field map was created by adding three loop coils at $z = -200$ cm, -150 cm, -140 cm, which corresponded to the Q7 location and either side of the yoke door respectively. The radius and current of these coils were adjusted to minimise the discrepancy with the Hall probe field map. This corrected the fringe field over the region that the muons passed through (radius < 4 cm), in a way that obeyed Maxwell’s equations.

The $P_\mu(0)$ values for the production and corrected field map are shown in Table 6.3. For the sets that used the silver target and a nominal beam profile, the $P_\mu(0)$ change was

³⁶In the DC tracking region where the field is $|B| = 2$ T, an NMR probe could be “locked”, allowing the Hall probes to be calibrated. This study determined that the raw Hall probe data required a correction between 0.85 mT and 0.95 mT. Since no NMR results were available for the fringe field region, the Hall probes cannot be trusted to better than 0.9 mT.

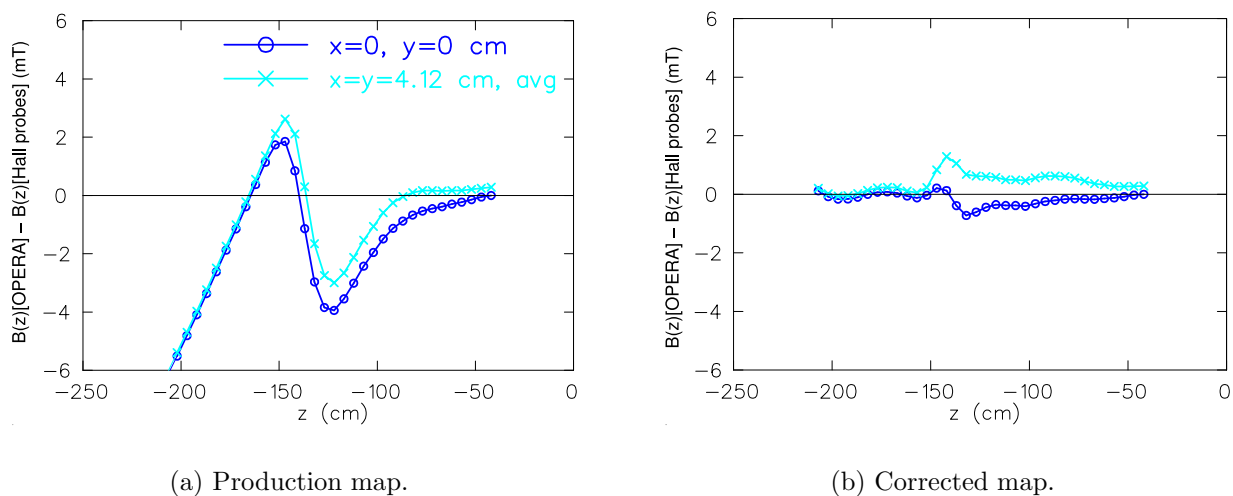


Figure 6.3: Difference in B_z between the magnetic field maps from OPERA and the Hall probes. Two comparisons are shown: the on-axis ($x = y = 0$) and an off-axis average of $x = \pm 4.12$ cm, $y = \pm 4.12$ cm. The corrected map has three current loops added. Muons start in the simulation at $z = -191.944$ cm.

between -9×10^{-4} (set 71) and -17×10^{-4} (set 75). For the aluminium target and nominal beam profile, the $P_\mu(0)$ change was between -20×10^{-4} (set 91) and -29×10^{-4} (set 83). The increased sensitivity for the aluminium target sets was due to the lower quality of the muon beam³⁷. The largest change in $P_\mu(0)$ for each target is a conservative estimate of the fringe field uncertainty: this would be 17×10^{-4} for the silver target, and 29×10^{-4} for the aluminium target. However, it will be shown that correcting $P_\mu(0)$ and then evaluating uncertainties based on the corrected map will allow the absolute polarisation to be known with greater precision.

The steered beam profiles were more sensitive to the field map. ΔP_μ^{74-76} and ΔP_μ^{87-86} are shown in Table 6.4, where the production field map is seen to underestimate the differences, but the corrected map appears to overestimate by $(17 \pm 8) \times 10^{-4}$ for ΔP_μ^{74-76} , and by $(53 \pm 7) \times 10^{-4}$ for ΔP_μ^{87-86} . These discrepancies will be revisited in the next section.

³⁷For the data accumulated with the aluminium target, a vertical aperture was in place within the M13 beam line. As a result the slits and jaws at the frontend of M13 were opened wider, and the beam did not come to a complete focus at F3; muons with $y > 1.0$ cm at the TECs did not converge towards the solenoid's axis (see Fig. 5.2).

Table 6.3: $P_\mu(0)$ for different field maps. For the translated map, the entire field was moved by (0.18, 0.19) cm.

Set num.	Target	Description	Production $P_\mu(0)$	Corrected field map $P_\mu(0)$	
				No translation	Translated
68	Ag	Stopping distrib. peaked $\frac{1}{3}$ into target	0.9978	0.9965	0.9968
70	Ag	B = 1.96 T	0.9975	0.9962	0.9962
71	Ag	B = 2.04 T	0.9969	0.9960	0.9959
72	Ag	TECs-in, nominal beam	0.9947	0.9901	0.9898
74	Ag	Nominal A	0.9975	0.9965	0.9963
75	Ag	Nominal B	0.9977	0.9960	0.9965
76	Ag	Steered beam A	0.9922	0.9847	0.9886
83	Al	Downstream beam package in place	0.9978	0.9949	0.9958
84	Al	Nominal C	0.9977	0.9954	0.9960
86	Al	Steered beam B	0.9931	0.9842	0.9831
87	Al	Nominal D	0.9978	0.9954	0.9964
91	Al	Lower momentum I	0.9969	0.9949	0.9955
92	Al	Lower momentum II	0.9966	0.9945	0.9952
93	Al	Lower momentum III	0.9967	0.9947	0.9951

 Table 6.4: Difference in $P_\mu(0)$ between nominal and low polarisation sets.

Sets	$\Delta P_\mu(0)(\times 10^{-4})$	
	s74-s76	s87-s86
Data	101 ± 8	59 ± 7
Production simulation	53	47
Simulation with corrected field, no rotation/translation	118	112
Simulation with corrected field, translated by (0.18, 0.19) cm	77	133

The corrected map that was shown in Fig. 6.3(b) still contains discrepancies at the $\lesssim 1$ mT level, which is about the accuracy of the Hall probes. A systematic uncertainty due to uncertainties in the field map can be estimated by determining how much features at the 1 mT level affect $P_\mu(0)$. The three coils that were used to correct the map had their currents adjusted by 10%, and the resulting field maps are shown in Fig. 6.4. The beam profiles for sets 74 and 87, which are both nominal, had $P_\mu(0)$ values in the range $0.9961 \rightarrow 0.9968$ and $0.9950 \rightarrow 0.9958$ respectively. This suggests that the $P_\mu(0)$ uncertainty from the degree to which the corrected map matches the true field is $\pm 4 \times 10^{-4}$. The $P_\mu(0)$ values for the steered beam sets were in the range $0.9838 \rightarrow 0.9857$ ($\pm 11 \times 10^{-4}$, set 76), and $0.9826 \rightarrow 0.9862$ ($\pm 18 \times 10^{-4}$, set 86).

The alignment of the Hall probe mapping device was known to about 0.2 cm in x and y . The position of the muon beam inside the detector was sensitive to the alignment of the entire magnetic field map. On a set-by-set basis, a field translation was determined such that the data and simulation positions matched. On average, this required a translation of the entire map by (0.18, 0.19) cm. Although this translation was determined precisely, we cannot be sure that it was accurate for a number of reasons: first, the position of the internal muon beam was also sensitive to the solenoid's coil positions³⁸. Second, the field through the hole in the yoke should be constrained to have its symmetry axis through the centre of the hole. Third, the translation was determined from beam profiles that will later be shown to suffer from their own alignment uncertainties. Also the translation may be compensating for the residual discrepancies in the field map (see Fig. 6.3(b)).

The effect of the field translation on $P_\mu(0)$ is included in Table 6.3. For the nominal profiles, the largest $P_\mu(0)$ change for the silver target was 5×10^{-4} (set 75), and for the aluminium target it was 10×10^{-4} (set 87). The steered beam profiles were more sensitive, and the corresponding ΔP_μ^{74-76} and ΔP_μ^{87-86} results have been added to Table 6.4; after translating the field, ΔP_μ^{74-76} and ΔP_μ^{87-86} are still not matched in data and simulation.

This section has shown that only making changes to the fringe field map's shape and alignment cannot reproduce the difference in polarisation between sets with a nominal and a steered muon beam. The systematic uncertainties that were evaluated in this section will be included in a later summary.

³⁸A change in the solenoid coil positions by ≈ 1 cm caused the internal muon beam to move by about ≈ 0.3 cm. The coil positions were known to ≈ 0.2 cm[100].

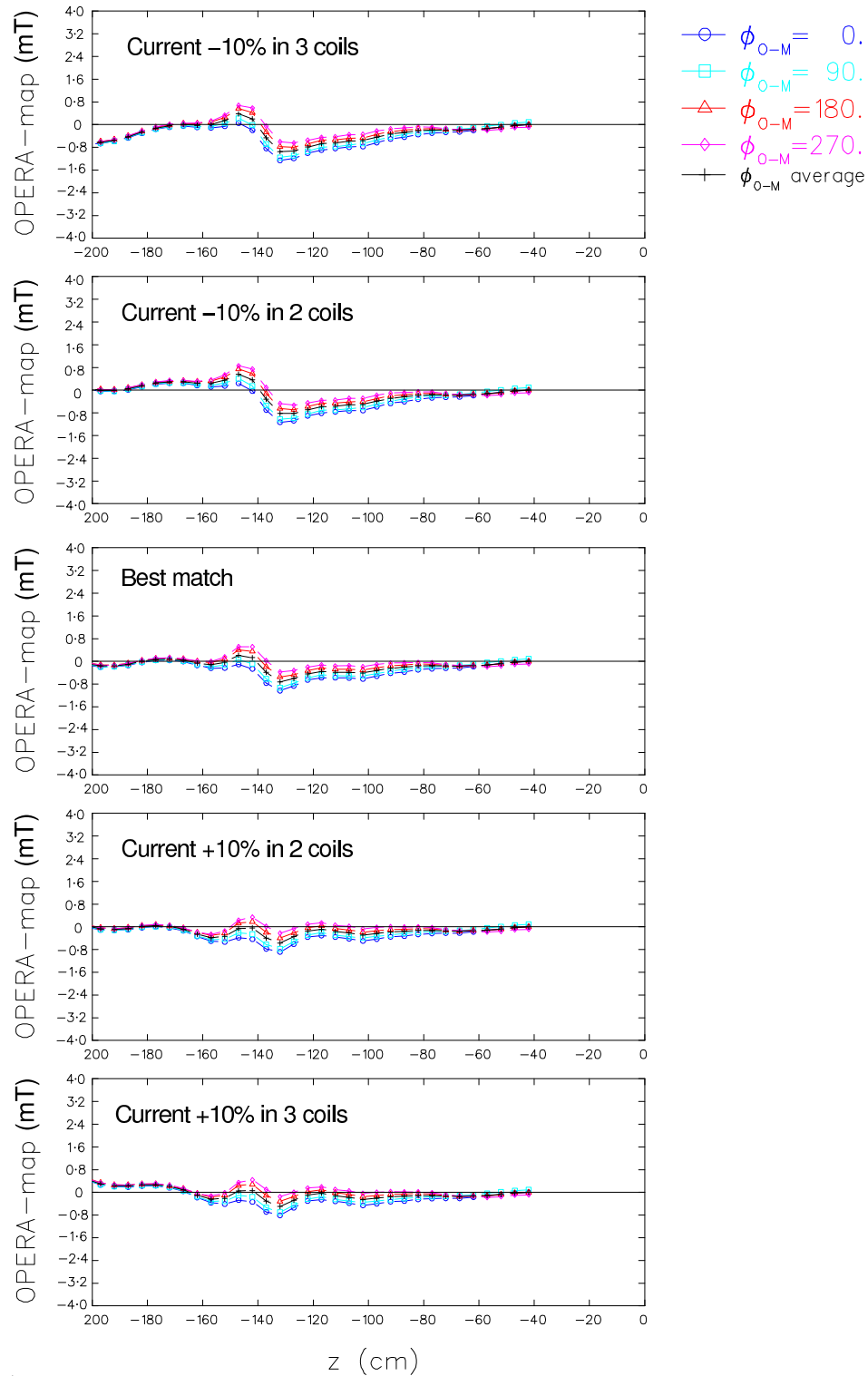


Figure 6.4: The difference between various fringe field maps and the Hall probe measurements. These maps have residual features at the ≈ 1 mT level. The differences are taken on-axis ($x = y = 0$ cm), and each line shows the discrepancy for a different azimuthal angle.

Muon beam average position and angle

A beam measurement was made with the TECs at the beginning and end of most data sets. The differences in the average positions and angles between these measurements are listed in Table 6.5, where changes of up to 0.18 cm in position and 3 mr in angle were observed. The origin may have been muon beam instability, a limitation in the reproducibility of the TECs, or an instability in the drift cell response.

Table 6.5: Muon beam differences for the beginning and end of set TEC measurements.

Set	Target	Description	$\Delta \langle x \rangle$ (cm)	$\Delta \langle y \rangle$ (cm)	$\Delta \langle \theta_x \rangle$ (mr)	$\Delta \langle \theta_y \rangle$ (mr)	ΔT^a (°C)
68	Ag	Stopping distrib. peaked $\frac{1}{3}$ into target	0.11	-0.05	0.2	-3.2	-0.3
70	Ag	B = 1.96 T	0.03	0.00	1.0	-0.4	-1.2
71	Ag	B = 2.04 T	0.09	-0.05	0.0	0.1	2.4
74	Ag	Nominal A ^b	-				
75	Ag	Nominal B	0.04	-0.10	-0.5	1.5	3.2
76	Ag	Steered beam	-0.04	-0.06	-0.6	1.9	1.3
83	Al	Downstream beam package in place	0.12	-0.09	0.6	0.7	-0.3
84	Al	Nominal C	0.18	-0.15	0.2	1.4	-0.4
86	Al	Steered beam B	0.04	-0.01	1.0	-0.01	-0.4
87	Al	Nominal D	0.13	-0.11	-0.1	0.7	-1.3
91/92/93	Al	Lower momentum ^b	-				

^a $\Delta T = T_{\text{end}} - T_{\text{start}}$. $\Delta T > 0$ indicates a temperature rise between measurements.

^b These sets only had one TEC measurement.

Muon beam instabilities were caused by a change in the proton beam upstream of the production target, or an instability in the M13 beam line elements. A special test displaced the proton beam at the production target by ± 0.1 cm vertically, which is a gross exaggeration of how much the beam could have moved during normal operation. The largest observed TEC changes in the muon beam were $\Delta \langle y \rangle = \pm 0.07$ cm in position and $\Delta \langle \theta_y \rangle = \pm 1.0$ mr in angle. These changes were not large enough to result in a significant muon beam instability from the proton beam steering.

The settings of the M13 beam line elements (*e.g.* quadrupoles, dipoles, slits, jaws, asymmetric currents for quadrupole steering) were all monitored with a slow controls system, and runs with an instability were eliminated (see Section 5.4). Sets 72 and 82 had the TECs in place throughout, and analysis of these sets found that the average muon beam position and angle were stable to < 0.02 cm and < 1 mr respectively (see Fig. 5.3). The muon beam mea-

surement from the wire chambers was used to monitor stability for the nominal sets, which did not have the TECs in place. The sensitivity of the internal beam to M13 instabilities was determined by adjusting the currents in each quadrupole and dipole by $\pm 5\%$. An examination of the internal beam found that the largest variations were 0.02 cm in position, which corresponded to a $P_\mu(0)$ change of 3×10^{-4} for the nominal beam tune. Instabilities in the muon beam do not explain the differences between beginning and end of set measurements in Table 6.5.

The space-time-relationship in the TEC drift cells depended on temperature. A change of $\pm 3^\circ\text{C}$ altered the average reconstructed positions by $\approx \pm 0.05$ cm, and angles by < 0.4 mr. The temperature differences in Table 6.5 are not correlated with the change in average beam parameters, ruling out temperature as the dominant cause of the beginning/end of set differences.

The insertion/removal of the TECs required the beam line elements to be switched off, and a breaking of the vacuum in the beam line, which then had to be pumped down again before the TECs could be used. This process exerted significant forces on the beam line components and the box containing the TECs, and these forces appear to be responsible for the measured variation in average initial position and angle.

There are now several degrees of freedom: the magnetic field translation (between (0, 0) cm and (0.18, 0.19) cm), the average position of the muon beam at the TECs (< 0.2 cm) and the average angle of the muon beam at the TECs (< 3 mr). Using these freedoms, an attempt was made to match all characteristics of the internal muon beam (as measured by the wire chambers) in data and simulation. The average muon positions from the simulation are compared to the data in Fig. 6.5. For the nominal sets, the position in data and simulation match after applying the magnetic field translation and a combination of changes in TEC position and angle, of which there are a family of possible solutions. The positions from the steered beam profiles do not match the data, and it is clear that the magnetic field and TECs would have to be modified well outside their uncertainties to achieve a match; this suggests that the shape of the fringe field map is still a problem for the steered beam profiles.

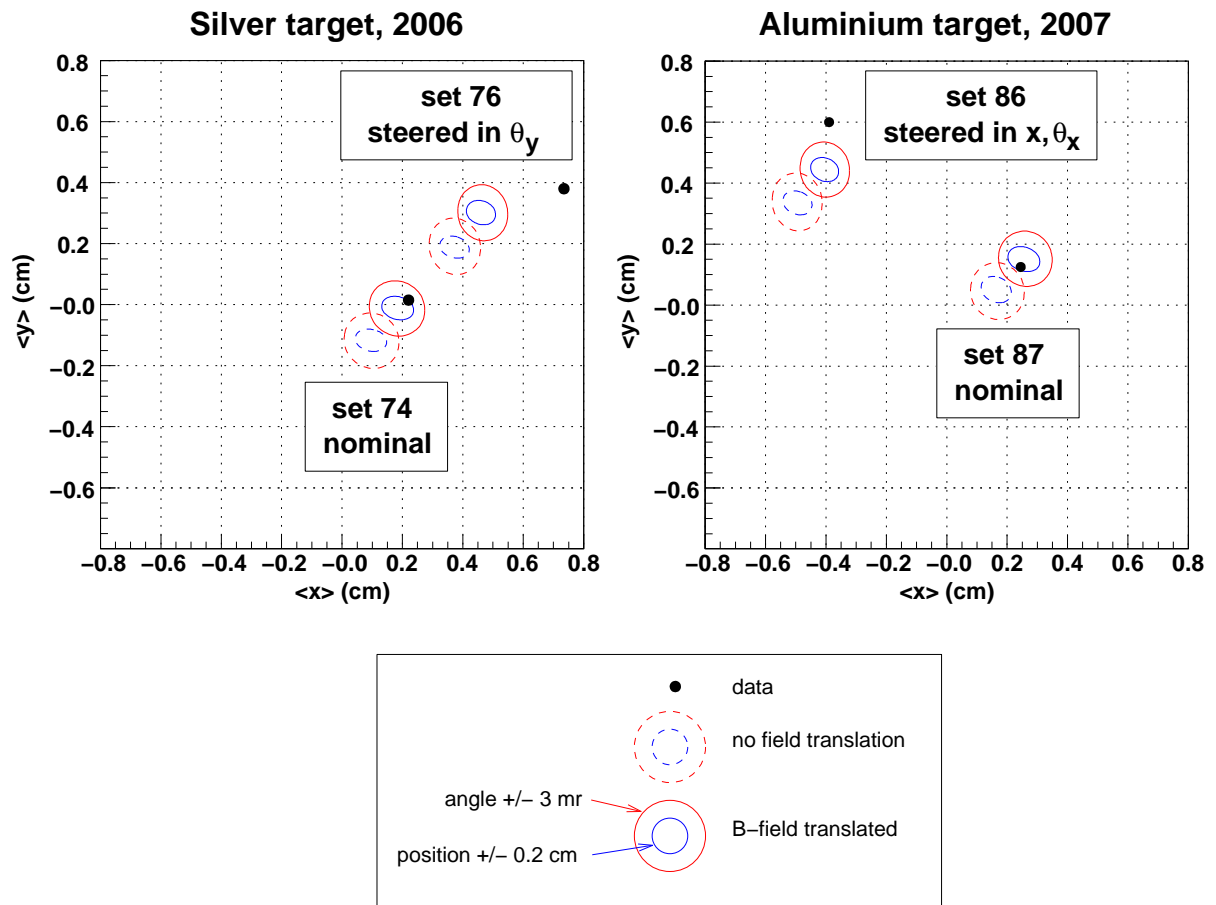


Figure 6.5: Internal muon beam position, as measured by the wire chambers. The spread in the simulation's position is due to uncertainties from the reproducibility of the TECs and the translation of the magnetic field.

The amplitude of muon beam oscillations in the detector, A , is shown in Fig. 6.6. This quantity is a measure of the transverse momentum, which is expected to be closely related to the polarisation since the momentum and spin vectors precess with almost the same frequency in magnetic fields (see Section 1.6.1). Note that the data-simulation match in A does not show a preference for the translation of the magnetic field. If the approximately quadratic dependence of $P_\mu(0)$ on A is extrapolated to match the data for sets 74 and 86, and interpolated for sets 76 and 87, then ΔP_μ^{74-76} and ΔP_μ^{87-86} from the simulation are

$$\Delta P_\mu^{74-76}(0) = (106 \pm 3) \times 10^{-4}, \quad (6.3)$$

$$\Delta P_\mu^{87-86}(0) = (73 \pm 2) \times 10^{-4}, \quad (6.4)$$

where the uncertainties here are from the spread in the data values, which are represented as a band in Fig. 6.6. Data and simulation now match for ΔP_μ^{74-76} , but ΔP_μ^{87-86} disagrees by 14×10^{-4} ; however, this is within the $\pm 18 \times 10^{-4}$ that was observed from field map variations at the 1 mT level in the previous section. Note that set 86 was carefully tuned to ensure the TECs did not clip the muon beam during measurement (otherwise this would have resulted in a different beam when the TECs were removed). Also, a simulation with the TECs in place confirmed that the same fraction of muons were missing the trigger scintillator for a nominal and the set 86 beam profile³⁹.

The ΔP_μ^{74-76} and ΔP_μ^{87-86} results suggest that $P_\mu(0)$ should be corrected so that A matches in data and simulation. For the nominal sets 74 and 87, this corresponds to correcting $P_\mu(0)$ from the ‘‘Translated’’ column of Table 6.3 by $+5 \times 10^{-4}$ and $+3 \times 10^{-4}$. However, this correction is determined using an imperfect fringe field map, and it should not be applied with confidence. Instead, the larger of the corrections ($\pm 5 \times 10^{-4}$) is taken as a contribution to the overall systematic uncertainty. There is also an uncertainty given by the range of $P_\mu(0)$ values from the magnetic field translation and TEC reproducibility. For the nominal sets 74 and 87, this is $\pm 7 \times 10^{-4}$ and $\pm 12 \times 10^{-4}$ respectively.

The phase and wavelength of the muon beam oscillations were also investigated. For the nominal beam, these were poorly determined and were not useful in making comparisons between data and simulation. The parameters for the steered beam sets were determined better, and are shown in Fig. 6.7. For set 76, a match in λ and ϕ is possible for a family of TEC displacements and rotations, but these parameters do not allow $P_\mu(0)$ to be constrained. For

³⁹Events were only analysed in the TECs if there was a signal at the trigger scintillator. There was a concern that the extra multiple scattering of the TECs would increase the emittance at the trigger scintillator, such that the muons would start to miss the trigger that would otherwise enter the spectrometer when the TECs were removed.

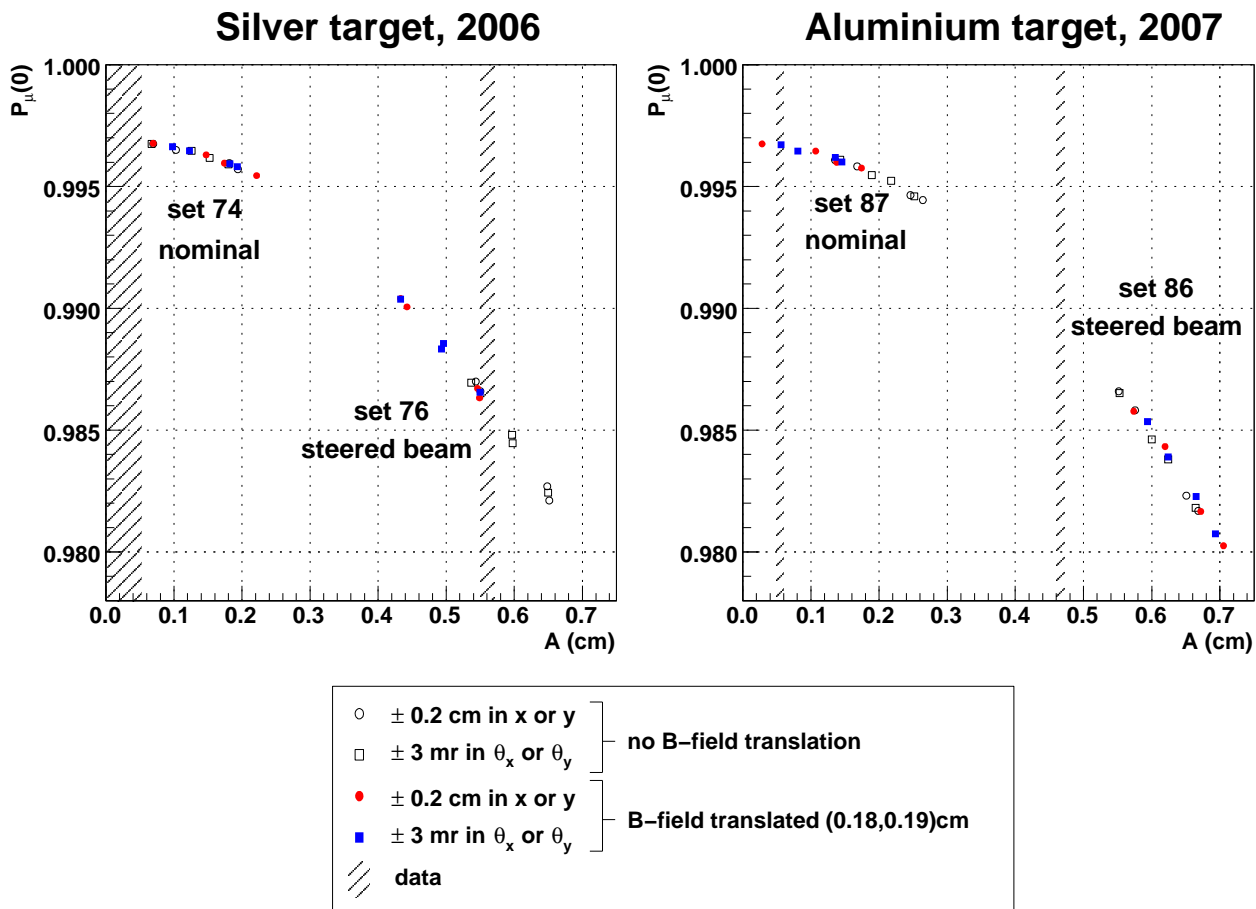


Figure 6.6: Amplitude of muon beam oscillations, A , and its relationship to $P_\mu(0)$. The combination of uncertainties in magnetic field translation and TEC position/angle allow an amplitude match to the data for two of the four sets.

set 86, there are discrepancies that confirm the earlier difficulties in matching A and ΔP_μ^{87-86} . The parameters that describe the decay of A and λ with z , A_d and λ_d in Eqs. (3.25), do not offer additional information since they are highly correlated with A and λ .

Lastly, the TEC sense planes that were used to measure the muon beam for sets 68 \rightarrow 72 were not calibrated, and instead the calibrations from another set of planes were used for the analysis. Section G.4 showed that the drift cell space-time-relationships and discriminator amplitude walk corrections were consistent between planes, but the wire time offset calibration found that the TEC modules had a rotation of between 7 – 12 mr within the TEC box. Since this angle was not determined for sets 68 \rightarrow 72, they suffer from an additional TEC angle uncertainty of ± 2.5 mr. This is smaller than the ± 3 mr used above to estimate the systematic uncertainty, so no further action has been taken.

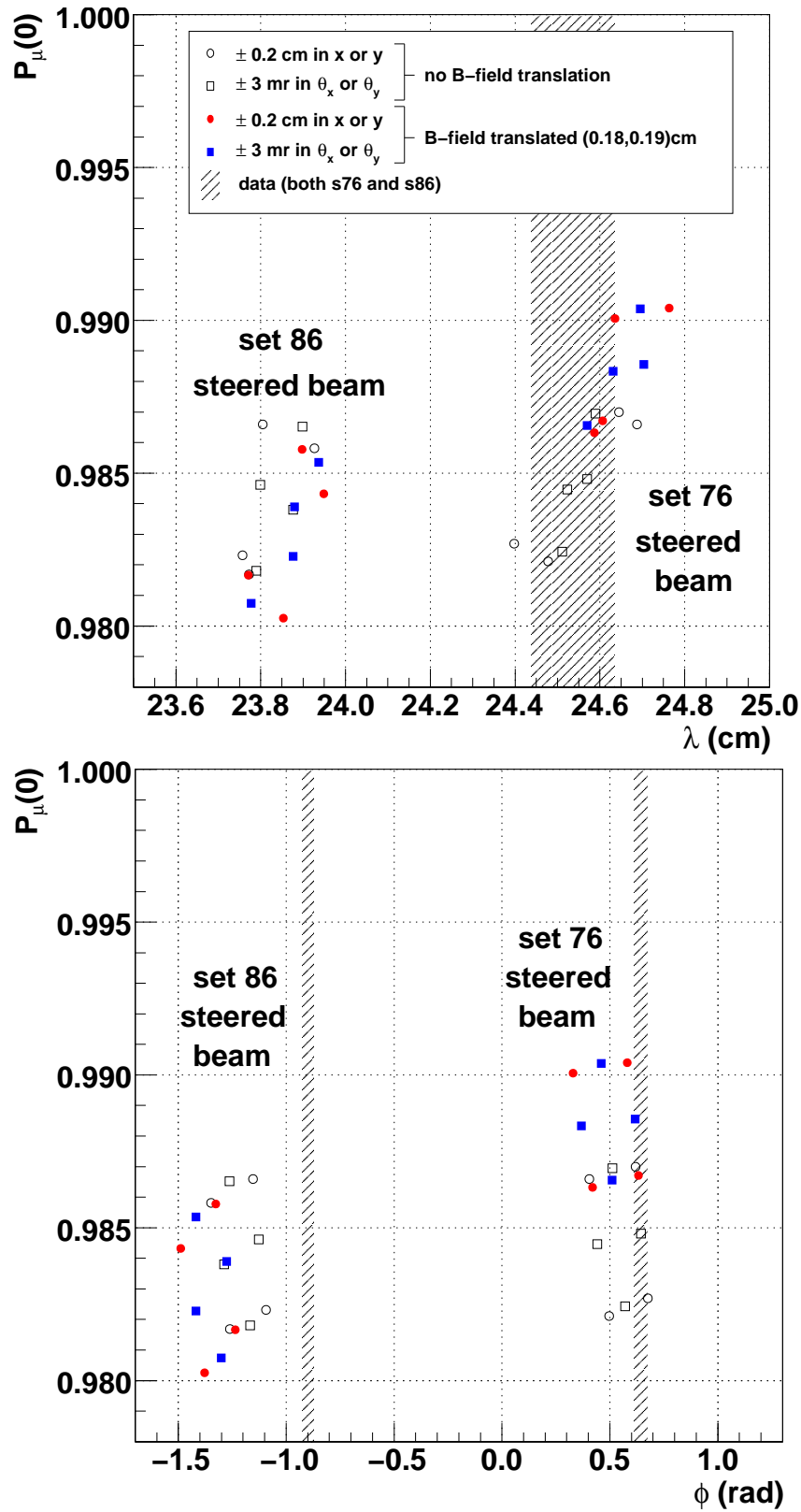


Figure 6.7: Wavelength (λ) and phase (ϕ) of the muon beam oscillations, for the steered sets.

Muon beam angular resolution

The muons were multiple scattered as they passed through the TECs. As a consequence, the RMS of the measured angles were larger than the beam would have been in the absence of the TECs. In order to correct for this, the RMS of the angles in each module were multiplied by a factor of $c_x = 63.91\%$ in the x -module, and $c_y = 47.95\%$ in the y -module. These were determined using a simulation of the TEC where the single hit efficiency was matched to the data.

The dependence of $P_\mu(0)$ on c_x and c_y is shown in Fig. 6.8, which demonstrates the sensitivity is independent of the beam profile. As a result, the choice of c_x and c_y has no bearing on the comparison of ΔP_μ^{74-76} and ΔP_μ^{87-86} between data and simulation. In addition, the internal beam measurement is barely affected by c_x and c_y , and their uncertainties can be treated as orthogonal to the $P_\mu^\pi \xi$ systematic uncertainties that have already been evaluated⁴⁰.

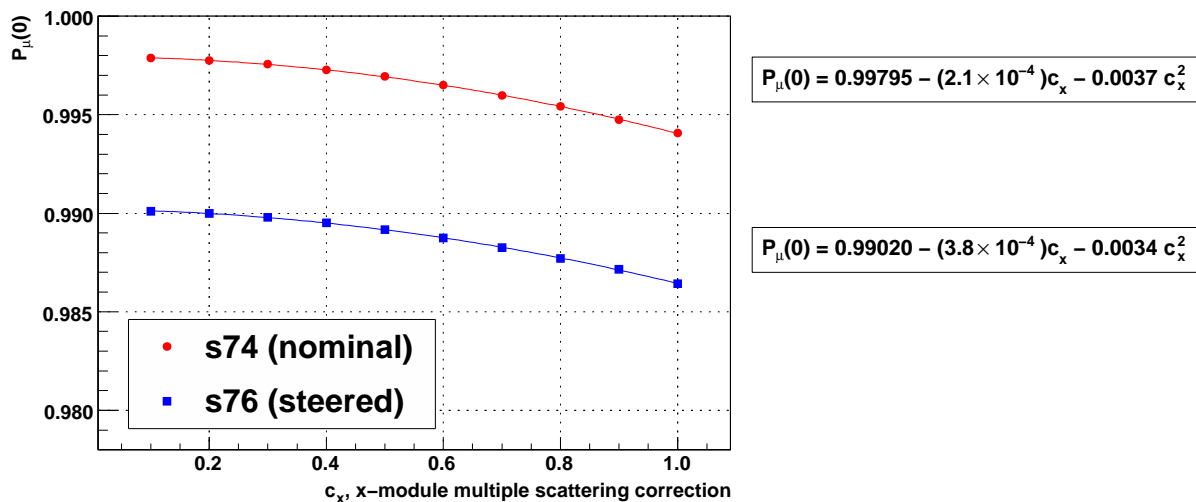


Figure 6.8: Sensitivity of $P_\mu(0)$ to c_x , the multiple scattering correction factor in the x -module. Note that the ratio $c_x/c_y = 63.91/47.95$ was maintained. The sensitivity of $P_\mu(0)$ is independent of the beam profile.

The values of c_x and c_y had negligible uncertainties from statistical precision and the degree to which the single hit efficiency matched the data. However, the tuning relied on accurate simulation of multiple scattering through small amounts of material (the TEC was equivalent to about 7 mg/cm^2 of material). Using the range of scattering distribution widths

⁴⁰If the ratio of c_x to c_y is maintained, and c_x is varied between 0 and 1, then the following muon beam changes are observed: the amplitude A changes by up to 0.03 cm for the steered sets, but there is no evidence of changes for the nominal sets. The wavelength and phase change by less than $< 0.4 \text{ cm}$ and 0.10 rad respectively, independent of profile. The largest position changes are 0.01 cm, again independent of profile.

from Table 6.2, this suggests that c_x and c_y were only accurate to about $\pm 30\%$. This introduces a significant systematic uncertainty of ${}^{+6.5}_{-10.8}$.

A review of the TEC analysis code concluded that the RMS of the angles could not be determined to better than 4 mr due to electronics noise (see Section G.3.4). In the x -module where the RMS was between ≈ 13 mr and ≈ 17 mr (depending on beam tune, age of sense planes, position of beam within TECs, preamplifier voltages), this introduced an uncertainty in the RMS of up to 30%. This is equivalent to only knowing c_x and c_y to 30%, which we already know corresponds to an uncertainty of ${}^{+6.5}_{-10.8}$.

The RMS of the angles depended on the age of the sense planes, for which no correction was made in the analysis. A systematic uncertainty can be estimated using set 72, where the TECs were in place for an entire set and the beam tune was nominal: $P_\mu(0)$ from a beam measurement at the end of the set was 8.0×10^{-4} less than at the beginning. Since the TECs were never allowed to age this much during normal operation, 8.0×10^{-4} is an upper limit on the systematic uncertainty from aging.

Lastly, the “tails” of the beam profile (x and y locations far from the core) had non-Gaussian angle distributions. These corresponded to x and y locations with less than $\approx 10\%$ of the peak number of muons. When these tails were eliminated, $P_\mu(0)$ for a nominal profile increased by 8.0×10^{-4} . By including the tails, the uncertainty on the simulation’s $P_\mu(0)$ value is certainly better than 8.0×10^{-4} .

Summary

The uncertainties for the muon beam and fringe field from this section are listed in Table 6.6, where the quadratic sum of the contributions implies a total systematic uncertainty of 21.5×10^{-4} . The contributions will now be briefly summarised.

For the nominal beam profiles, the difference in $P_\mu(0)$ between the production fringe field and a corrected map was 17×10^{-4} for the silver target, and 29×10^{-4} for the aluminium target. These values set an upper limit on the $P_\mu^\pi \xi$ uncertainty due to the field map.

Variations in the corrected field map at the level of $\lesssim 1$ mT suggest that $P_\mu(0)$ for the nominal sets is accurate to $\pm 4 \times 10^{-4}$. The corresponding uncertainties for the steered sets are $\pm 11 \times 10^{-4}$ for set 76, and $\pm 18 \times 10^{-4}$ for set 86.

The muon beam measurement from the wire chambers suggests that the magnetic field map needs to be translated by (0.18, 0.19) cm to match the position of the beam in data and simulation. However, we cannot fully justify this field translation, so it is treated as a degree of freedom. The measurement of the muon beam by the TECs appears to be limited by the reproducibility of the TEC box within the M13 beam line. (Instabilities from the

proton beam, M13 beam line elements and temperature variations within the drift cell were ruled out as the dominant cause of measurement instability.) This limits the accuracy of a TEC beam measurement to < 0.2 cm in position, and < 3 mr in angle, providing additional degrees of freedom.

The freedom in field translation and TEC position/angle were used to attempt a simultaneous data-simulation match of the internal muon beam. The positions of the nominal sets could be matched, but only after translating the entire field map in (x, y) by $(0.18, 0.19)$ cm. The other internal beam parameters had no clear preference for a field translation. If the amplitudes were matched, then ΔP_μ^{74-76} and ΔP_μ^{87-86} agreed in data and simulation, within the earlier field map uncertainties. The uncertainty from not matching A in data and simulation for the nominal maps was estimated as 5×10^{-4} for both targets. The uncertainties from the translation of the field map and the TEC reproducibility were $\pm 7 \times 10^{-4}$ for the silver target and $\pm 12 \times 10^{-4}$ for the aluminium target.

The RMS of the angles at the TECs could only be determined with a limited precision of ≈ 4 mr, which introduced a systematic uncertainty of ${}_{-10.8}^{+6.5}$. (The average of the upper and lower bounds has been entered into Table 6.6.) No correction was made for the aging of the sense planes, which resulted in a systematic error in the RMS of the angles; an upper limit on this error was determined as 8.0×10^{-4} . A correction was applied to the RMS of the angles due to multiple scattering within the TECs. This was accurate to about 30% due to uncertainties in the simulation of multiple scattering through small amounts of material, and introduced a systematic uncertainty of ${}_{-10.8}^{+6.5}$. (Again, the average of these bounds appears in Table 6.6.) Lastly, the analysis imposed a Gaussian form on the distribution of the angles, but this was not appropriate in the tails of the beam profile. An upper limit on the error introduced was determined as 8.0×10^{-4} .

Table 6.6: Summary of muon beam and fringe field uncertainties, for sets with a nominal beam tune.

Description	Systematic uncertainty ($\times 10^{-4}$)	
	Silver target	Aluminium target
Upper limit from field	< 17	< 29
1 mT fringe field variations	4	4
Internal beam A not matched	5	5
Translation of field and TEC uncertainties	7	12
Quadratic sum	9.5	13.6
Simulation of multiple scattering ^a		8.7
Noise from TEC electronics ^a		8.7
Aging of TEC sense planes		< 8
Non-Gaussian tails of beam profile		< 8
Quadratic sum		16.7

^a These uncertainties were asymmetric. In this table, the average value of the upper and lower bounds has been used.

6.3.3 Stopping material

About 80% of the muons stopped in a metal target, which also served as the shared cathode foil for the proportional chambers PC6 and PC7 (see Fig. 2.14). Events were only accepted if the muon produced a signal in PC6, but not in PC7. Muons that stopped in the PC6 gas or wires were then removed by cutting on the muon pulse width in the chamber (see Section 3.3.3). This selected a clean sample of muons that stopped in the metal foil.

The weighted asymmetry was constructed according to the method described in Section 3.6, and each data set was fit with

$$P_\mu(t) = P_\mu(0) \exp(-\lambda t). \quad (6.5)$$

The results for the time range ($1.05 < t < 9.00$) μs are shown in Table 6.7. A weighted average of these relaxation rates finds $\lambda_{\text{Ag}} = (0.909 \pm 0.075) \text{ ms}^{-1}$ and $\lambda_{\text{Al}} = (1.301 \pm 0.076) \text{ ms}^{-1}$.

Table 6.7: Relaxation rate λ for each data set. $P_\mu(t) = P_\mu(0) \exp(-\lambda t)$ has been fit over the nominal time range of ($1.05 < t < 9.00$) μs .

Set num.	Target	Description	λ	Fit quality	
			(ms^{-1})	χ^2/ndof	confidence
68	Ag	Stopping distrib. peaked $\frac{1}{3}$ into target	0.94 ± 0.22	$18.5 / 20 = 0.93$	0.552
70	Ag	B = 1.96 T	0.85 ± 0.18	$15.3 / 20 = 0.77$	0.757
71	Ag	B = 2.04 T	1.08 ± 0.19	$26.7 / 20 = 1.34$	0.143
72	Ag	TECs-in, nominal beam	0.95 ± 0.19	$27.5 / 20 = 1.38$	0.121
74	Ag	Nominal A	1.18 ± 0.23	$18.3 / 20 = 0.92$	0.566
75	Ag	Nominal B	0.98 ± 0.18	$16.2 / 20 = 0.81$	0.706
76	Ag	Steered beam A	0.38 ± 0.21	$13.8 / 20 = 0.69$	0.841
82	Al	TECs-in, spread beam	1.24 ± 0.22	$10.1 / 20 = 0.50$	0.967
83	Al	Downstream beam package in place	1.50 ± 0.19	$28.1 / 20 = 1.40$	0.108
84	Al	Nominal C	1.12 ± 0.20	$31.9 / 20 = 1.60$	0.044
86	Al	Steered beam B	1.28 ± 0.17	$22.5 / 20 = 1.12$	0.315
87	Al	Nominal D	1.24 ± 0.19	$13.6 / 20 = 0.68$	0.852
91	Al	Lower momentum I	1.67 ± 0.36	$21.7 / 20 = 1.08$	0.359
92	Al	Lower momentum II	1.34 ± 0.31	$13.3 / 20 = 0.66$	0.865
93	Al	Lower momentum III	1.27 ± 0.24	$13.0 / 20 = 0.65$	0.876

The simulation used preliminary values of $\lambda_{\text{Ag}} = 0.732 \text{ ms}^{-1}$ and $\lambda_{\text{Al}} = 1.169 \text{ ms}^{-1}$. The weighted asymmetry analysis was applied to the simulation, and found $\lambda_{\text{Ag}} = (0.580 \pm$

$0.087) \text{ ms}^{-1}$ and $\lambda_{\text{Al}} = (1.068 \pm 0.087) \text{ ms}^{-1}$, using the nominal time range of $(1.05 < t < 9.00) \mu\text{s}$. These results are 1.7σ and 1.2σ below the true values in the simulation, indicating a bias in analysis. A separate investigation found that an unbiased muon lifetime measurement required a time fiducial of $(2.00 < t < 9.00) \mu\text{s}$. If the asymmetry analysis is applied to the simulation with a lower time cut of $2.00 \mu\text{s}$, then $\lambda_{\text{Ag}} = (0.59 \pm 0.12) \text{ ms}^{-1}$ and $\lambda_{\text{Al}} = (1.15 \pm 0.12) \text{ ms}^{-1}$, which are consistent with the true values.

The data were reanalysed with the time range of $(2.00 < t < 9.00) \mu\text{s}$, yielding the experiment's most precise unbiased results for the relaxation rates,

$$\lambda_{\text{Ag}} = (1.01 \pm 0.10) \text{ ms}^{-1}, \quad (6.6)$$

$$\lambda_{\text{Al}} = (1.20 \pm 0.10) \text{ ms}^{-1}. \quad (6.7)$$

Note that these are consistent with the $\mu^+\text{SR}$ results from Section H.8:

$$\lambda_{\text{Ag}} = (0.9 \pm 0.2 \text{ (stat.)} \pm 0.2 \text{ (syst.)}) \text{ ms}^{-1}, \quad (6.8)$$

$$\lambda_{\text{Al}} = (1.3 \pm 0.2 \text{ (stat.)} \pm 0.3 \text{ (syst.)}) \text{ ms}^{-1}. \quad (6.9)$$

The simulation used an inaccurate λ value, and as a result $P_\mu^\pi \xi$ must be corrected. The effect on the spectrum of a change in λ can be calculated using

$$\frac{\int_{t_1}^{t_2} N(t) \cdot P_\mu(0) \exp(-\lambda_1 t) dt}{\int_{t_1}^{t_2} N(t) dt} - \frac{\int_{t_1}^{t_2} N(t) \cdot P_\mu(0) \exp(-\lambda_2 t) dt}{\int_{t_1}^{t_2} N(t) dt}, \quad (6.10)$$

where $N(t) = N(0) \exp(-t/\tau_\mu)$ and τ_μ is the muon lifetime, and λ_1 and λ_2 are the relaxation rates between which the correction is being made. The corrections to the simulation's P_μ are then -8.4×10^{-4} and -0.9×10^{-4} for silver and aluminium respectively. The statistical uncertainty in determining λ from the data causes a P_μ uncertainty of 3.0×10^{-4} for both targets, again using Eq. (6.10).

The simulation found that about 0.2% of muons entered PC7, but did not have enough energy to produce a signal. The depolarisation within the PC gas ($\text{CF}_4/\text{isobutane}$) and wires was about 3%. The systematic uncertainty due to these stops is therefore $\approx 0.2\% \times 3\% = 0.6 \times 10^{-4}$, which is negligible.

6.3.4 Background muon contamination

In the previous $P_\mu^\pi \xi$ analysis, the number of muons downstream of the stopping target did not agree in the data and simulation; this is demonstrated in Fig. 6.9(a). The stopping distributions were consistent if pion decays were simulated in the upstream “beam package” area. Improvements in the current analysis have removed most of the discrepancy, without having to include the additional pion decays; the modern agreement is demonstrated in Fig. 6.9(b).

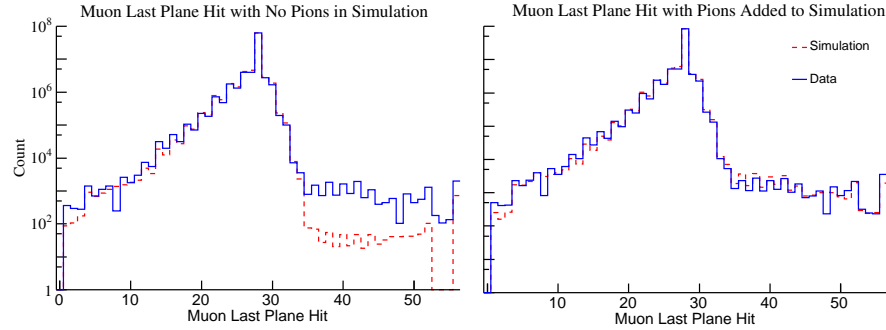
The residual discrepancy in Fig. 6.9(b) introduced an uncertainty in the muon stopping distribution, which must be matched to prevent a bias in the muon polarisation, since high angle muons that undergo more depolarisation are preferentially stopped further upstream. Specifically, the simulation needed an extra 1.9 mg/cm^2 of material to match the stopping distribution in the data (see Section 2.11), and we could not be sure whether this was justified. Fortunately the effect on the polarisation was minimal: including an extra 1.9 mg/cm^2 in the simulation introduced a systematic uncertainty of just 1×10^{-4} for all the beam profiles except set 72 (TECs-in), which had an uncertainty of 4×10^{-4} .

6.3.5 Beam intensity

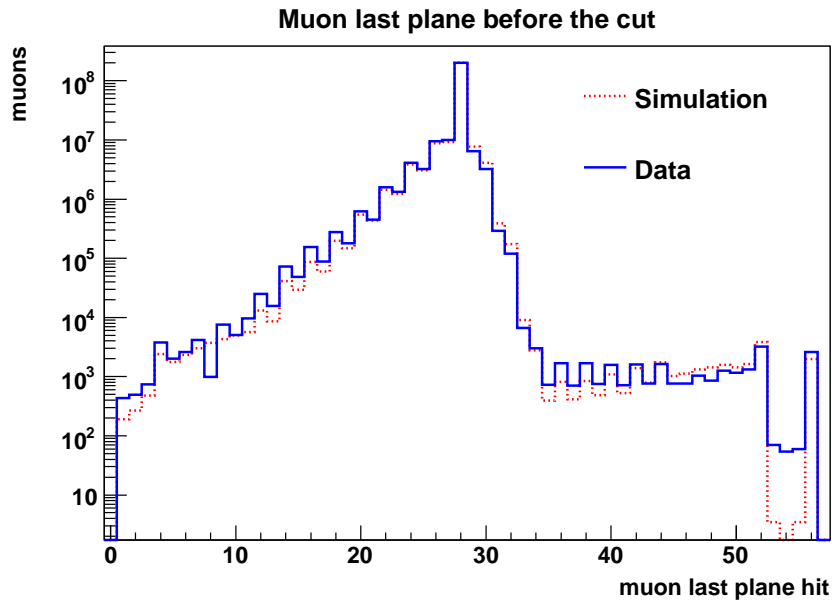
If a particle (muon or beam positron) arrived within 200 ns of the muon’s decay, its signals were potentially confused with the decay positron. The beam positron systematic uncertainty was previously estimated by exaggerating the rate by a factor of 60. This changed $P_\mu^\pi \xi$ by $(-5 \pm 7) \times 10^{-4}$, *before* scaling down (*i.e.* the systematic uncertainty was actually 60 times smaller)[18]. This confirmed that beam positrons were removed from the analysis with sufficient accuracy.

TODO: find out why we even have a problem at high muon rates. Then use Rob’s non-zero sensitivity (Sec 8.6) but with modern Rmu evaluation, until Anthony does the proper evaluation using different Michel spectra for each event type. PARK: probably need to tabulate Rmu properly according to section 8.6 of Robs thesis.

- Main effect of muon rate is that increasing channel makes worse beam profile. This systematic covers effect on reconstruction



(a) Comparison of muon stopping distribution from the previous analysis (originally Fig. 6.9 from Ref. [57]). The mismatch between data and simulation is resolved by adding muons from pion decays in the M13 beam line.



(b) The same figure re-made for the current analysis. In this figure there are no additional pion decays added.

Figure 6.9: Background muon contamination in the two $P_{\mu}^{\pi} \xi$ analyses.